A Maverick Asymmetrical Backbone with Distinct Flanked Twist Angles Modulating the Molecular Aggregation and Crystallinity for High Performance Nonfullerene Solar Cells

Xunchang Wang, Zurong Du, Keke Dou, Huanxiang Jiang, Chenglin Gao, Liangliang Han, and Renqiang Yang*

In this work, a new asymmetrical backbone thienobenzodithiophene (TBD) containing four aromatic rings is designed, and then four polymers PTBD-BZ, PTBD-BDD, PTBD-FBT, and PTBD-Tz are synthesized. The planar and high degree of π-conjugation configuration can guarantee effective charge carrier transport and the distinct flanked dihedral angles between the TBD core and conjugated side chain can subtly regulate the molecular aggregation and crystallinity. The four polymer/3,9-bis(2-methylene-(3-(1,1-dicyanomethylene)-indanone)-5,5,11,11-tetrakis(4-hexylphenyl)-dithieno[2,3-d:2′,3′-d′]-s-indaceno[1,2-b:5,6-b′]-dithiophene (ITIC) blending films exhibit predominantly face-on orientation. The photovoltaic devices based on wide bandgap polymers PTBD-BZ and PTBD-BDD achieve power conversion efficiencies (PCEs) as high as 12.02% and 11.39% without any post-treatment. For the medium bandgap polymers PTBD-FBT and PTBD-Tz, the devices also show good PCEs of 10.18% and 11.02% with high V_{OC} of 0.94 and 1.02 V, respectively, which indicates simultaneously achieving a $V_{OC} > 1$ V and a high J_{SC} is feasible to further improve the PSCs' performance by modifying this new backbone. This work reveals that the versatile asymmetric backbone is an excellent moiety to construct light-harvesting copolymers and to modulate the microstructure for highly efficient PSCs.

1. Introduction

Polymer solar cells (PSCs), which can be fabricated into large-area device by low-cost solution processing methods, are a very promising light-harvesting technology and renewable energy source.[1–4] The past few years have witnessed the rapid progress of nonfullerene n-type acceptors and the PCE of nonfullerene-based PSCs devices have already surpassed 13% for single-junction devices.[5–9] To achieve efficient nonfullerene PSCs and mature fully from research into cost effective products, it is of critical importance not only to design high-performance small molecular acceptors (SMAs), but also to develop matching donor polymers, as well as to deeply understand the mechanism of the coordinated microstructure interactions between donor and acceptor components.[10–15]

Key and fundamental strategies for designing high-effciency nonfullerene PSC devices are absorption spectrum and energy level. The donor and acceptor components should possess complementary absorptions and high extinction coefficient to enhance light harvesting to achieve high J_{SC}.[16,17] The matching energy levels are crucial for donor and acceptor to ensure efficient driving force of exciton dissociation, to minimize voltage loss and thus to guarantee high V_{OC}. However, the troublesome tradeoff between high V_{OC} and J_{SC} is inevitable which is the big challenge for further improving the PSCs performance.[18,19] In addition, the most difficult and complicated problem is how to precisely modulate the microstructure of the blending system. The donor should exhibit good morphology compatibility with the acceptor, including suitable crystallinity, appropriate aggregation, face-on orientation, and moderate domain size, and thus to achieve excellent charge transport and high fill factor (FF).[20–22] Therefore, establishing universal and general guideline of rational designing compatible D/A structure is extremely urgent and important for nonfullerene PSCs.

Benzo[1,2-b:4,5-b′]dithiophene (BDT) and dithieno[2,3-d:2′,3′-d′]benzo[1,2-b:4,5-b′]dithiophene (DTBDT) are the dominant backbones for donor polymers because of their planar framework, showing the most high performance in PSCs.[23–30] Most researchers focus on the side chain engineering of BDT- and DTBDT-based polymers and demonstrate that optimized side-chain can easily control polymer packing

X. Wang, Z. Du, K. Dou, H. Jiang, C. Gao, Dr. L. Han, Prof. R. Yang
CAS Key Laboratory of Bio-based Materials
Qingdao Institute of Bioenergy and Bioprocess Technology
Chinese Academy of Sciences
Qingdao 266101, China
E-mail: yangrq@qibebt.ac.cn
X. Wang, Z. Du, H. Jiang
University of Chinese Academy of Sciences
Beijing 100049, China

The ORCID identification number(s) for the author(s) of this article can be found under https://doi.org/10.1002/aenm.201802530.

and bulk heterojunction (BHJ) morphology.[31–33] However, the backbone configuration would also be a key factor to improve the performance. In spite that DTBDT with extended π-conjugation can effectively improve its charge carrier transport when compared with BDT, the torsion angles between the flanked substituent side chain and planar backbone of DTBDT are much larger than that of BDT unit, which might strongly reduce the aggregation of DTBDT-based polymer.[29,34] Furthermore, the conjugated length of backbone can precisely lessen the steric hindrance of the adjacent side chain to regulate the crystallinity and intermolecular π–π stacking, resulting in better polymer-small molecular acceptor miscibility and microstructures.[35] Our recent work demonstrated that it is not necessary for high-performance nonfullerene polymer solar cells to possess highly ordered microstructures in the blending films.[36] During the drying process of the active layer, the polymer with high crystalline behavior will have a tendency to form large domain size, leading to terrible miscibility. In other word, polymers with moderate crystallinity could be more compatible with small molecular acceptor to form excellent morphology. According to the above illustrations, it is crucial to design the polymers with suitable crystallinity for nonfullerene PSCs. Thus, it is feasible that extending the conjugation of BDT backbone from one end to obtain an asymmetric backbone can not only improve its charge carrier transport, but also modulate the twist angles and the steric hindrance of the adjacent side chains, further resulting in well balanced molecular packing and aggregation. However, the asymmetric planar aromatic backbone has seldomly been used for donor polymers, probably due to the preconception that efficient D–A copolymers should be regioregular. In addition, compared with side chain engineering, subtle backbone change, such as configuration and conformation alteration, can dramatically influence the exciton dissociation and transport for the PSCs.[37] In this work, we report a new synthesis method of asymmetric building block TBD containing four fused rings with longer backbone length than BDT unit and shorter than DTBDT unit. An effective side chain modification method, alkylthiolation, was utilized to fine-tune the highest occupied molecular orbital (HOMO)/lowest unoccupied molecular orbital (LUMO) energy levels and thus increase V_{OC}.[38] Then a series of copolymers were prepared with different acceptor units (BZ, BDD, FBT, and Tz) to investegate the effects of asymmetric backbone for different D–A systems in detail. The four new polymers were named PTBD-BZ, PTBD-BDD, PTBD-FBT, and PTBD-Tz, which were obtained through palladium-catalyzed Stille polycondensation. The compatibility with ITIC was then investigated by using as-cast PSCs to analyze the effects of asymmetric backbone and to identify promising donor materials for nonfullerene PSCs.[39] Surprisingly, it was found that the asymmetric backbone had dramatic influence on polymer geometric configuration with two distinct flanked twist angles, which can subtly regulate the molecular packing and morphology. All the polymers/ ITIC blending films exhibited predominantly face-on orientation and moderate crystallinity as well as slightly weak aggregation. As a result, all the devices based on these blendings obtained impressive PCEs. In particular, the PTBD-BZ- and PTBD-BDD-based devices showed the PCE of 12.02% and 11.39% without any processing additives or post-treatment. In addition, for PTBD-FBT and PTBD-Tz, their devices also gave 10.18% and 11.02% PCEs

with high V_{OC} of 0.94 and 1.02 V, respectively. Thus, these results not only reveal a newly promising asymmetric donor building block to construct D-A copolymers, but also demonstrate an effective strategy employing asymmetric backbone to modulate the microstructure for highly efficient PSCs.

2. Results and Discussion

The target copolymers are shown in **Figure 1** and the detailed synthetic procedure for the monomers and polymers are provided in the Supporting Information (Scheme S1). The key intermediate compound **2** was prepared from compound **1** through a cyclization reaction in 60% yield. The trimethyltin chloride was introduced by a lithium–hydrogen exchange reaction on compound **3**, resulting in **M1** in 72% yield. The BZ-, BDD-, and FBT-based polymers were obtained through Stille polymerization using $Pd_2(dba)_3$ and $P(o\text{-tol})_3$ as catalysts. The Tz-based polymer was synthesized by Stille-coupling polycondensation using another catalyst $Pd(PPh_3)_4$. All the copolymers exhibited good solubility in common organic solvents such as chloroform, toluene, and chlorobenzene. The number-average molecular weight (M_n) and polydispersity index (PDI) were measured by high temperature gel permeation chromatography (GPC) using trichlorobenzene as eluent in order to hinder the aggregation of polymers in low temperature that can highly likely influence accuracy of M_n. The polymers PTBD-BZ, PTBD-BDD, PTBD-FBT, and PTBD-Tz have M_n of 18.9, 40.5, 19.9, and 43.0 kDa with corresponding PDIs of 2.85, 3.24, 2.14, and 2.15, respectively. Thermogravimetric analysis indicated that all the copolymers are stable up to 320 °C, which is sufficiently high for PSCs application (Figure S1, Supporting Information).

Theoretical calculations were performed to investigate the effect of the asymmetric backbone on molecular geometry and electronic structure by using the density functional theory (DFT) with the B3LYP/6–31G (d,p) basis set. To facilitate the calculation, side alkyl chains were simplify to methyl groups. As illustrated in **Figure 2**, for the donor unit, the same two substituted side chains extending the conjugated system bonded the geometry of TBD moiety, and the optimized geometries of the four polymers revealed that the dihedral angles of both sides between the planar TBD core and conjugated side chain were different ranging from 59° to 78°, which was ascribed to the asymmetric backbone. The moderate twisting geometry was beneficial to improve the solubility and inhibit strong aggregation of the corresponding polymers. Furthermore, the two distinct dihedrals could promote the polymers to produce well-controlled crystallinity, which can ensure appropriate phase separation and good miscibility when blending with the ITIC. The dihedrals within BZ, FBT, and Tz acceptor units were much smaller than those within BDD unit. The small dihedrals within BZ and FBT were ascribed to the noncovalent attractive interactions between strong polar fluorine atoms and sulfur atoms in neighboring thiophene rings.[40] The planar Tz unit resulted from the thiazole ring reducing the steric hindrance with TT central units.[41] For the electron distribution, it can be observed that the HOMO surface of the polymers delocalize in both TBD and accept units and the LUMO surface of the polymers mainly localize in the acceptor units. The theoretical calculation data of the energy level was summarized in **Table 1**.

ADVANCED
SCIENCE NEWS

www.advancedsciencenews.com

ADVANCED
ENERGY
MATERIALS

www.advenergymat.de
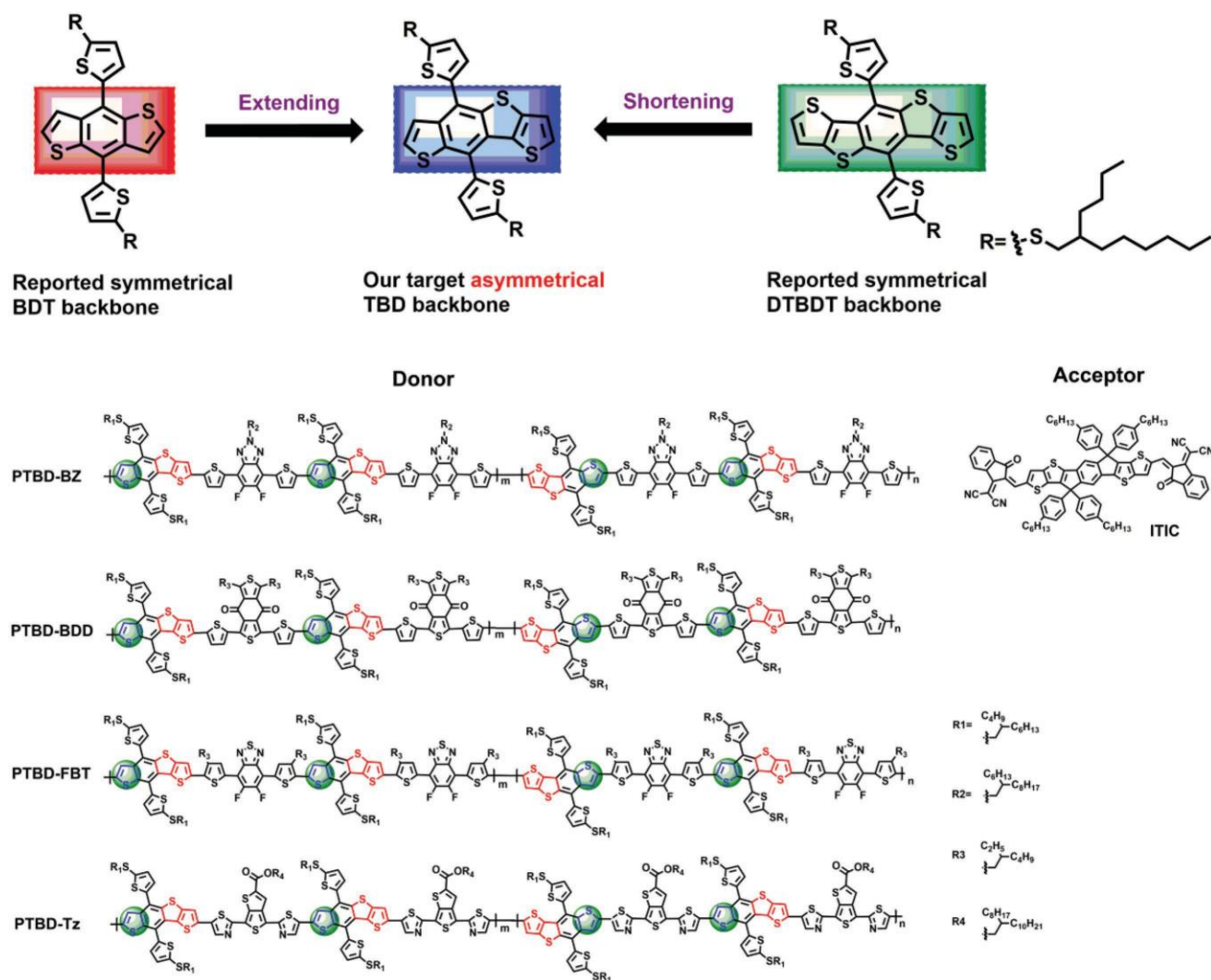
Figure 1. Chemical structures of target polymers of the two different repeating units with different regioregularity and acceptor.

To obtain insight into the crystallinity and molecular orientation of the pure TBD-based polymer films, grazing-incidence wide-angle X-ray scattering (GIWAXS) method was carried out. **Figure 3**a showed the 2D GIWAXS patterns of the neat polymers and the corresponding scattering profiles in the in-plane (IP) and out-of-plane (OOP) direction were displayed in Figure 3b. All the neat films in IP direction showed sharp diffraction peaks (100) with a medium intensity diffraction peak (010) in OOP direction, indicating predominant face-on oriented π–π stacking in pure polymers. Note that the π–π stacking distance of PTBD-BZ, PTBD-BDD, PTBD-FBT, and PTBD-Tz were 3.60, 3.76, 3.68, and 3.59 Å^{-1}, respectively. The lamellar stacking peaks for PTBD-BZ, PTBD-BDD, PTBD-FBT, and PTBD-Tz were recorded at q_{xy} = 2.90, 2.68, 3.03, and 2.57 nm^{-1}, corresponding to lamellar stacking distances of 22.36, 24.21, 21.39, and 25.21 Å, respectively. By combining the DFT and GIWAXS results, the similar geometry, crystallinity (strong (100) peak and moderate (010) peak) and molecular orientation of the TBD-based polymers could be attributed to the asymmetric TBD backbone with moderate twisting geometry, which

can inhibit strong aggregation of the corresponding polymers. The modulating molecular aggregation and crystallinity, as well as face on orientation of the TBD-based polymers may have great advantage in nonfullerene PSCs.

The UV–vis absorption spectra of the four polymers in both dilute chlorobenzene solution and thin film at ambient temperature were shown in **Figure 4**, and the related properties were summarized in Table 1. One can observe that in solution and film, the four polymers exhibited broad absorption, without a obviously bathochromic shift of their maximum absorption, implying effective aggregation of these polymer chains formed even in solution phase. In the solid states, the well-defined absorption peaks were displayed with an additional vibronic peak in the long wavelength region, indicating strong intermolecular interaction and effective stacking of the polymer chains. To further investigate the aggregation behavior of the four polymers in solution, the temperature-dependent UV–vis absorption spectra in dilute chlorobenzene solution (10^{-5} m) were monitored starting from room temperature with heating to 100 °C (Figure S2, Supporting Information). When the

ADVANCED
SCIENCE NEWS

www.advancedsciencenews.com

ADVANCED
ENERGY
MATERIALS

www.advenergymat.de
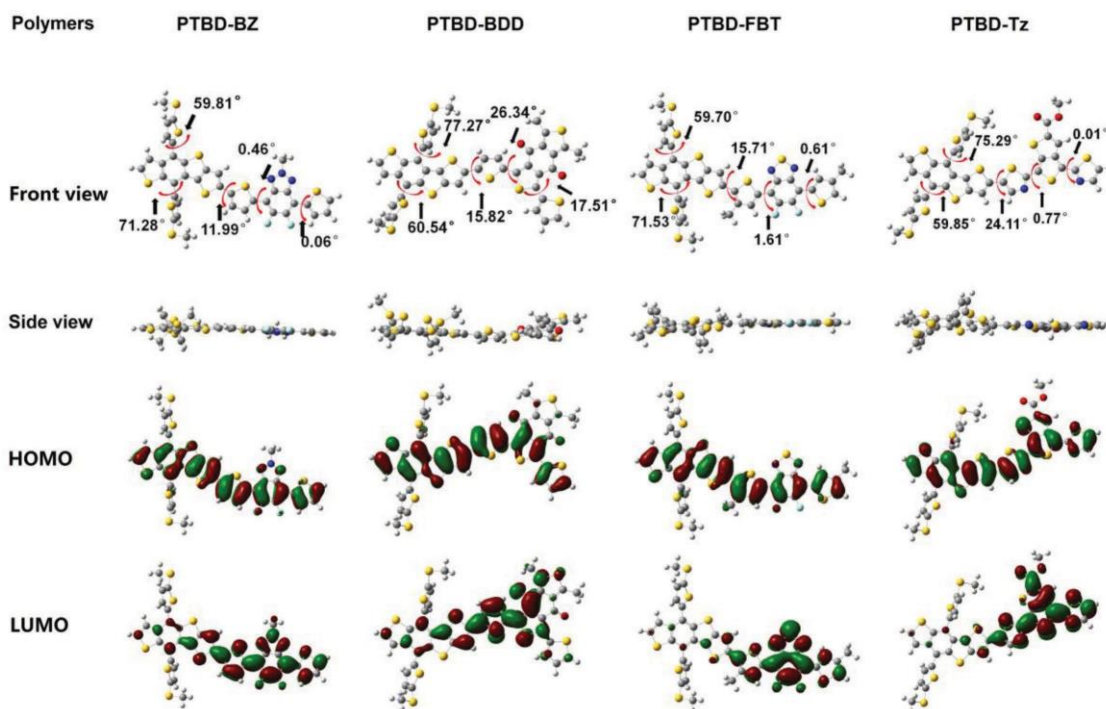
Figure 2. Simulated molecular geometries and frontier molecular orbital distribution of the four polymers.

solution temperature increased, the spectra of PTBD-BDD and PTBD-FBT exhibited notable blueshifts, declining absorption intensity, and narrowing of the absorption bands, which revealed the dissociation of aggregation. When the temperature increased to 100 °C, the aggregation was almost completely broken. In contrast, the solution of polymers PTBD-BZ and PTBD-Tz still exhibited the distinct and sharp shoulder at the long wavelength region and inconspicuous blueshifts even if the temperature was increased to 100 °C, indicating much stronger aggregation and intermolecular stacking even in hot dilute solution for the two polymers. In order to understand the aggregation variation by changing the backbone from symmetric (BDT) to asymmetric (TBD), we compared the temperature-dependent spectra of polymer PTBD-BDD with that of the classical polymer PBT1-BO.[42] The PBT1-BO still shows strong aggregation even the temperature at 70 °C while the aggregation of PTBD-BDD is almost broken, indicating the asymmetric backbone with the distinct flanked twist angles could slightly weaken the aggregation. The optical band gaps (E_g^{opt}) of the four

polymers, PTBD-BZ, PTBD-BDD, PTBD-FBT, and PTBD-Tz, estimated from the onset of the film absorption edges, were 1.90, 1.78, 1.68, and 1.72 eV according to the equation $E_g^{opt} = 1240/\lambda_{onset}$, respectively.

Cyclic voltammetry (CV) was performed to investigate the electrochemical properties of the polymers and ITIC.[43] The onset oxidation and reduction potentials of all the materials can be estimated in Figure S3 (Supporting Information), and the HOMO and LUMO energy levels were calculated according to the equations $E_{(HOMO/LUMO)} = -(E_{ox/red} + 4.39)$ (eV), which were summarized in Table 1. It was found that the polymer PTBD-BZ exhibited quasi reversible oxidation process in the electrochemical experiments, while all the other three polymers showed irreversible oxidation property.[44–46] The E_{HOMO} values of PTBD-BZ, PTBD-BDD, PTBD-FBT, PTBD-Tz, and ITIC were −5.40, −5.46, −5.42, −5.52 and −5.53 eV, respectively. The deep HOMO levels (≤−5.40 eV) of these polymers could improve their stability under ambient conditions.[47] In addition, the lower HOMO of the polymer as donor is beneficial for

Table 1. Photophysical and electrochemical parameters of the four polymers.

Polymer	λ_{max} [nm]		λ_{edge}[a] [nm]	HOMO[b] [eV]	LUMO[b] [eV]	HOMO[c] [eV]	LUMO[c] [eV]	E_g^{opt}[d] [eV]
	Solution	Film						
PTBD-BZ	554,596	557,601	652	−5.40	−3.59	−5.02	−2.36	1.90
PTBD-BDD	574,616	576,621	695	−5.46	−3.72	−5.17	−2.44	1.78
PTBD-FBT	606,651	620,663	738	−5.42	−3.77	−5.08	−2.81	1.68
PTBD-Tz	610,651	607,660	721	−5.52	3.86	−5.21	2.74	−1.72

[a] Evaluated from the absorption band edge of the polymer film; [b] Measured by cyclic voltammetry; [c] Calculated from DFT; [d] Calculated from the absorption edge of the polymer films: $E_g^{opt} = 1240/\lambda_{edge}$.
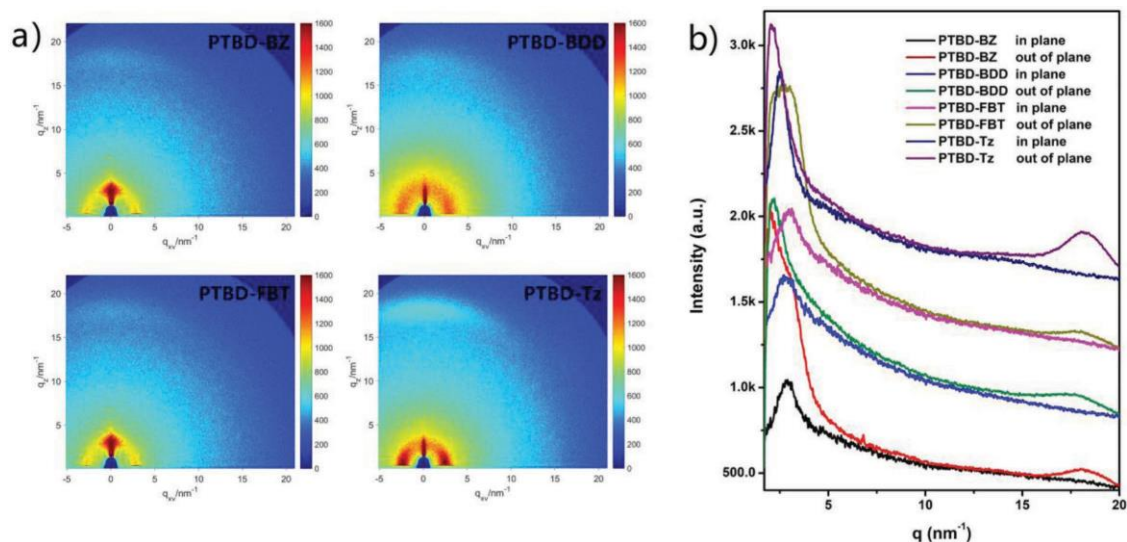
Figure 3. a) 2D GIWAXS patterns and b) the line-cut profiles for pure polymer films.

obtaining higher V_{OC} of the PSCs, since the V_{OC} is proportional to the difference between the LUMO of the electron acceptor and the HOMO of the electron donor. **Figure 5**a showed the energy level diagrams of the polymers and ITIC for a clear comparison. It should be noticed that the $\otimes E_{HOMO}$ between the polymer donors and ITIC acceptor is quite small: 0.13, 0.07, 0.11, and 0.01 eV for PTBD-BZ, PTBD-BDD, PTBD-FBT, and PTBD-Tz, respectively.

To explore the photoinduced exciton dissociation and charge transfer behavior with the small offset of the $\otimes E_{HOMO}$, the photoluminescence (PL) spectra of the pristine copolymers, ITIC and their blend films were examined. All the films were fabricated from CB solution and two excitation wavelengths, 600 and 720 nm, were applied for polymer/ITIC films with 1:1 (wt/wt) blend compositions. Figure S4 (Supporting Information) showed that the PL emission of the four polymers exhibited strong signals in the range of 620 to 750 nm when excited at 600 nm, which were located in the absorption range of ITIC. Whereas for the blend films, the PL emissions were almost completely quenched, suggesting efficient electron transfer from the polymers donors to the ITIC acceptor. However, the polymer PTBD-Tz exhibited the lowest quenching efficiency,

which could influence the charge separation in its device. Figure 5b shows the PL spectra of ITIC and the blending films when excited at 720 nm. The PL emission of ITIC was dramatically quenched by mixing with each of the four polymers, which indicated that the blend films would exhibit noteworthy hole transfer from the ITIC acceptor to the polymer donor. However, the emission quench efficiency of PTBD-Tz was still the weakest, implying that the negative $\otimes E_{HOMO}$ would have detrimental effect on charge transfer, leading to increasing charge recombination before they reach the electrodes.

The PSCs devices were fabricated with a conventional structure of indium tin oxide (ITO)/poly(3,4-ethylenedioxythiophene)-poly(styrene sulfonate) (PEDOT:PSS)/active layer/perylene diimide functionalized with amino N-oxide (PDINO)/Al to evaluate the photovoltaic performance. The devices were optimized by different conditions, such as donor/acceptor weight ratio, additive, thermal annealing (TA) and solvent vapor annealing (SVA). All the devices were obtained using CB as a processing solvent and the temperature was confirmed to be 130 °C for 10 min under TA treatment. In addition, when SVA treatment was performed, the active layer was completely immersed in CB vapor atmosphere
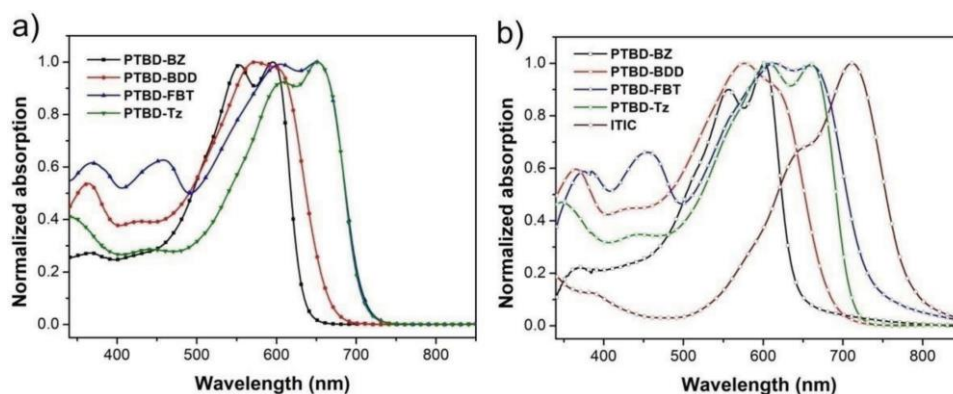
Figure 4. Normalized UV–vis absorption spectra of the polymers a) in solution, b) in thin films together with ITIC.

1802530 (5 of 11)
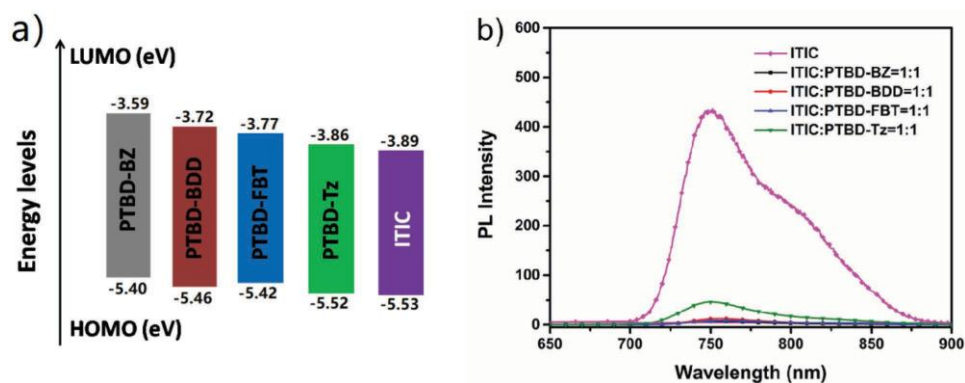
Figure 5. a) Energy level diagram of the polymer donors and ITIC acceptor, b) photoluminescence spectra of ITIC and its blend films with the four polymers.

(140 °C) for 5 min. The detailed device optimization data was summarized in the Supporting Information (Table S1). The corresponding current density–voltage (J–V) curves of the optimal devices based on four polymers were shown in **Figure 6**a, and their photovoltaic parameters were summarized in **Table 2**. Notably, the wide bandgap polymers PTBD-BZ- and PTBD-BDD-based PSCs did not need any complicated post treatments such as processing additives and annealing. Consequently, the optimal PTBD-BZ:ITIC based device yielded a PCE of 12.02% with a J_{SC} of 18.43 mA cm^{-2}, a V_{OC} of 0.915 V, and an FF of 71.30%. A comparable PCE of 11.39% was obtained for the PTBD-BDD:ITIC based PSCs, with a decent J_{SC} of 17.32 mA cm^{-2}, a high V_{OC} of 0.989 V, and an FF of 66.55%. The higher V_{OC} (0.989 V) of the PTBD-BDD-based PSC than that of the PTBD-BZ-based PSC (0.915 V) was resulted from the lower-lying HOMO level of PTBD-BDD (Table 1). These results indicated that it is possible to achieve a delicate and precise balance between the V_{OC} (<1 V) and J_{SC} in this case if the V_{OC} is dramatically improved by lowering the HOMO level of the donor, while J_{SC} can be maintained at almost the same value.

For medium bandgap polymer:ITIC system, the PTBD-Tz gave a high V_{OC} of 1.025 V, accompanying the J_{SC} still at a very high level (17.54 mA cm^{-2}). Both the polymers PTBD-FBT and PTBD-Tz exhibited excellent PCE of 10.18% and 11.02%, respectively. These results indicated again that it is promising to simultaneously achieve high V_{OC} (>1 V) and J_{SC} through rational backbone design. In addition, it was noted that the devices based on four polymers with the asymmetric main-chain obtain decent FF, which might be ascribed to the good microstructure of the blend films. Compared with the well-known polymer J61-based PSC, the polymer PTBD-BZ-based PSC exhibited rather higher FF (71.30%), suggesting that preferable charge transport channels or phase separation should be formed in the active layer arising from the asymmetric fused rings possessing the longer backbone size than BDT unit.[26] It can be concluded that selecting appropriate D-building block to modulate energy level and increase D/A compatibility should be crucial for PSCs, and thus the asymmetric backbone TBD would be a promising moiety to construct highly efficient donor polymers.
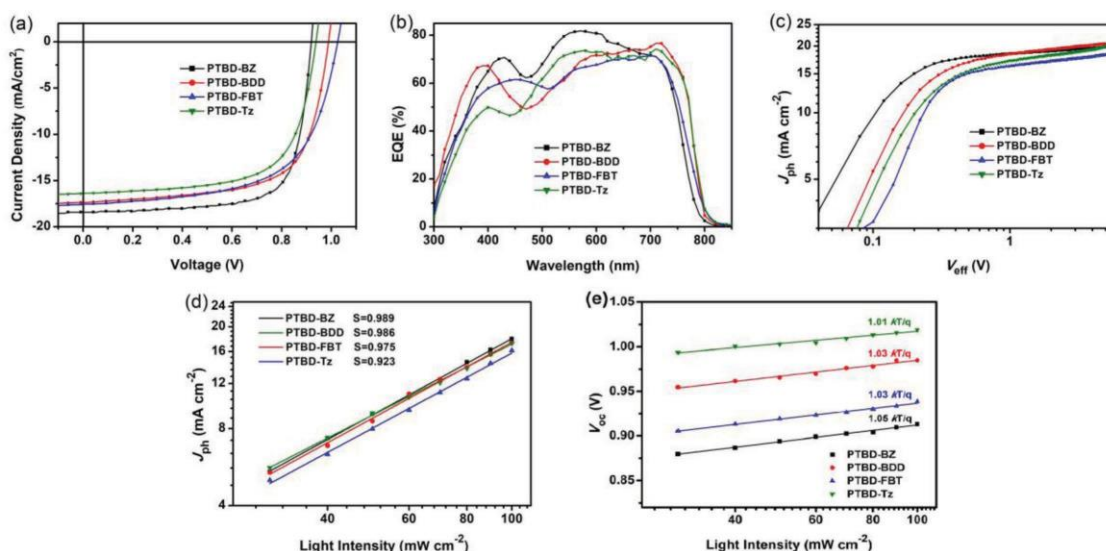
Figure 6. a) The J–V characteristics of the optimized PSCs based on the polymers as donor and ITIC as acceptor under the illumination of AM1.5G, 100 mW cm^{-2}, b) EQE curves of the corresponding PSCs, c) J_{ph} versus V_{eff} curves of the four optimized BHJ devices, d) J_{ph}–P_{light} curves of the optimized devices, e) light intensity dependence of V_{OC} of the optimized devices.

Table 2. Photovoltaic parameters of the PSCs based on polymer:ITIC, under the illumination of AM 1.5G, 100 mW cm^{-2}.

Polymers	V_{OC} [V]	J_{SC} [mA cm^{-2}]	J_{SC}^{EQE} [mA cm^{-2}]	FF [%]	PCE[a] [%]	μ_h [cm^2 V^{-1} s^{-1}]	μ_e [cm^2 V^{-1} s^{-1}]	P_{dis}
PTBD-BZ	0.915	18.43	17.67	71.30	12.02 (11.92)	2.15×10^{-4}	2.54 × 10^{-4}	94.1
PTBD-BDD	0.989	17.32	17.28	66.55	11.39 (11.21)	1.16 ×10^{-4}	1.57 × 10^{-4}	86.4
PTBD-FBT	0.939	16.36	16.09	66.28	10.18 (9.80)	0.79×10^{-4}	2.10 × 10^{-4}	92.3
PTBD-Tz	1.025	17.54	17.09	61.27	11.02 (10.83)	1.01×10^{-5}	6.29 × 10^{-5}	87.7

[a]The best PCE values, and the average PCE values are provided in parentheses from 15 devices.

The external quantum effciency (EQE) spectra of the corresponding PSC devices based on the four polymers were shown in Figure 6b. These devices exhibited a broad photon response ranging from 300 to 800 nm, which were attributed to the intrinsic absorption characteristics of both polymer donor and ITIC acceptor. The PTBD-BZ-based PSCs showed the high EQE values (over 60%) from 500 to 700 nm with the maximum EQE value of 80.9% at ≈550 nm. As a result, PTBD-BZ-based devices yielded the highest J_{SC}. In addition, although the HOMO level of PTBD-Tz was close to ITIC ($\otimes E_{HOMO} = 0.01$), the PTBD-Tz-based device still displayed very high EQE values from 400 to 750 nm, indicating that the charge separation was only slightly affected and electron/hole transfer between acceptor and donor was still quite efficient. This phenomenon further demonstrates that it is feasible to overcome the tradeoff between V_{OC} and J_{SC}, simultaneously obtaining high J_{SC} and boosting V_{OC} over 1 V. The current densities integrated from the EQEs curves were consistent well with those obtained from J–V measurements, with a deviation less than 5%.

The charge transport property in device is a crucial factor for photovoltaic performance, here space-charge-limited current (SCLC) method was used to evaluate the hole mobility of pure polymers, and hole and electron mobility of the blending films. The detail measurement results were summarized in Table 2 and Table S2 (Supporting Information), and were displayed in Figures S5–S7 (Supporting Information). As shown in Table S2 (Supporting Information), the hole mobility of the pure polymers with this asymmetric TBD backbone were 8.26×10^{-4}, 1.48×10^{-3}, 6.13×10^{-4} and 1.96×10^{-4} cm^2 V^{-1} s^{-1} for PTBD-BZ, PTBD-BDD, PTBD-FBT, and PTBD-Tz, respectively, which were comparable to other reported BDT- and DTBDT-based polymers. On the other hand, the balance between the hole and electron mobility in the active layer is important for improving the FF and PCE.[48] Interestingly, the PTBD-BZ-based device showed the highest μ_h and μ_e of 2.15×10^{-4} and 2.54×10^{-4} cm^2 V^{-1} s^{-1} with balanced μ_e/μ_h of 1.18, which should be one important reason for its high J_{SC} and FF. Conversely, PTBD-Tz gave the lowest FF, probably due to the large unbalanced carrier transport ($\mu_e/\mu_h = 6.22$).

Meanwhile, the relationship between the photocurrent density (J_{ph}) and the effective voltage (V_{eff}) was investigated to study the exciton generation and charge dissociation. For the devices under optimized condition, the photocurrent density is calculated by: $J_{ph} = J_L - J_D$, where J_L and J_D are the current densities under illumination and in the dark, respectively. Then, V_{eff} was estimated by the following equation: $V_{eff} = V_o - V_a$, where V_o is the voltage when J_{ph} equals zero (i.e., $J_L = J_D$) and V_a is the applied voltage. As shown in Figure 6c, the sufficiently negative effective bias ($V_{eff} > 3$ V) was applied to ensure exciton generation rate reaching maximum (G_{max}) and the photocurrent density reaching saturation, implying that almost all excitons were dissociated and photogenerated charge carriers were completely collected by the electrodes. The values of the J_{sat} for the optimized devices were determined to be 19.58, 20.05, 17.73, and 20.01 mA cm^{-2} for PTBD-BZ, PTBD-BDD, PTBD-FBT, and PTBD-Tz, respectively, which meant that the light absorption of PTBD-FBT-based device is the lowest. The charge dissociation probability (P_{dis}) is defined as J_{ph}/J_{sat} and the corresponding values were summarized in the Table 2. Under short-circuit conditions, the P_{dis} for the devices of PTBD-BDD:ITIC and PTBD-Tz:ITIC were 86.4% and 87.7%, lower than that of PTBD-BZ:ITIC and PTBD-FBT:ITIC, indicating that the exciton dissociation was suppressed in the PTBD-BDD- and PTBD-Tz-based PSCs. Subsequently, the dependence of J_{SC} on light intensity was performed to investigate the charge recombination behavior. The correlation between the value of J_{ph} and light intensity can depict as $J_{ph} \propto P^S$, where P is the light intensity and S is a power-law scaling exponent and should be unity when the bimolecular recombination is negligible. As shown in Figure 6d, the relative S values were approximately fitted to be 0.989, 0.986, and 0.975, respectively, implying there was less bimolecular recombination for the optimized PSCs based on PTBD-BZ, PTBD-BDD, and PTBD-FBT. However, the PTBD-Tz-based device gave S value of 0.923, suggesting serious bimolecular recombination was occurred under short-circuit conditions, which should be another key factor for PTBD-Tz to obtain low FF. Figure 6e exhibits the V_{OC} plotted with respect to incident light intensity which can be expressed as $V_{OC} \propto nKT/q$ ln(P_{light}), where k is the Boltzmann constant, T is temperature, and q is the elementary charge. Generally, bimolecular recombination will dominate recombination process when the n is close to one. In contrast, if the n is close to two, the trap-assisted recombination will be the main process. As seen from Figure 6e, the parameter (n) is about 1.05, 1.03, 1.03, and 1.01 for the optimized PSCs based on PTBD-BZ, PTBD-BDD, PTBD-FBT, and PTBD-Tz, respectively, indicating that the bimolecular recombination was incontrovertibly the main process and the trap-assisted recombination could be negligible for these PTBD-based devices.

The TEM measurements were carried out to provide further insights into the compatible D/A morphology of the active layers. Three different processing conditions were applied to probe the self-aggregation and phase separation, that is, without post-treatment, TA and SVA. As we know, the traditional bulk heterojunction contains three phase separation regions, pure polymer, pure ITIC and polymer-ITIC mixing region.[49] The optimal extent of polymer–ITIC mixing and the domain
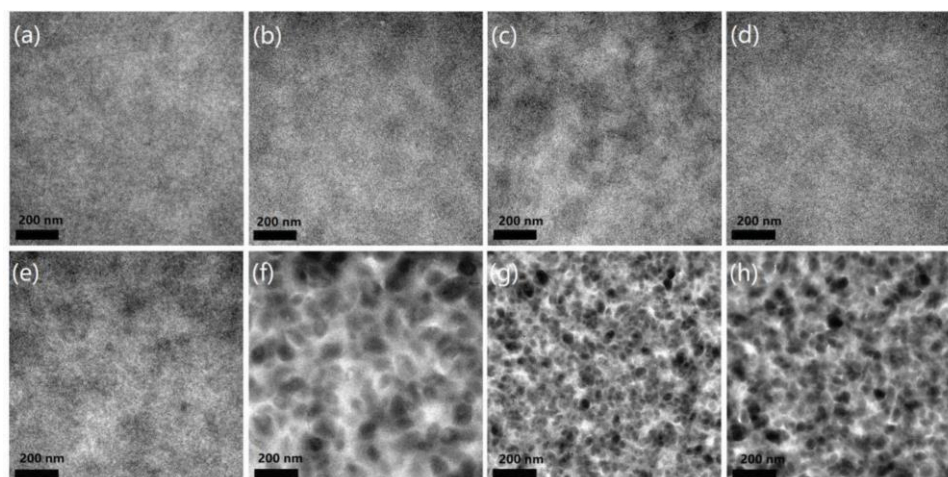
Figure 7. The TEM images for the blend films with different conditions. a) PTBD-BZ:ITIC film, b) PTBD-BDD:ITIC film, c) PTBD-FBT:ITIC film, and d) PTBD-Tz:ITIC film without post treatment. e) PTBD-BZ:ITIC film, f) PTBD-BDD:ITIC film, g) PTBD-FBT:ITIC film, and h) PTBD-Tz:ITIC film with solvent vapor annealing treatment.

continuity need to be well balanced. An increase in polymer aggregation signifies a reduce in the number of polymer backbones available to interact with ITIC small molecules. The larger degree of polymer-ITIC mixing points to a smaller extent of phase separation, leading to easy charge recombination. For the four polymers/ITIC blends, when the films were prepared by spin-coating without post treatment (**Figure 7**a–d), the polymers and ITIC mixed well without any obvious self-aggregation, which was probably due to the asymmetric backbone reducing the ordered microstructure. The less compact intermolecular packing and diminished steric hindrance induced ITIC to infiltrate into the void of polymer interchains, resulting in good miscibility. As shown in Figure 7a and Figure S8a (Supporting Information), the morphology of the blending PTBD-BZ/ITIC with TA treatment was almost same compared with that without any post treatment. When the SVA treatment was used (Figure 7e), the phase separation between PTBD-BZ and ITIC was slightly larger and the interpenetrating network was more obvious, which would repress the exciton recombination and benefit to charge transport, as a result, the FF was increased to 72.45% (Table S1, Supporting Information). It is noted that when the SVA treatment was used to process the PTBD-BDD/ITIC film, severe aggregation with the domain size > 50 nm was observed (Figure 7f), which was detrimental to the transport of charge carriers. As a result, the device showed relatively low FF. In contrast, when the blending PTBD-FBT/ITIC and PTBD-Tz/ITIC were prepared by using SVA treatment, phase separation in the blend became noteworthy and the moderate size aggregation was formed, which can lead to improved J_{SC} and FF (Figure 7g,h). Therefore, we believe that the SVA treatment is an effective method to modulate the aggregation property for TBD-based blend films, and it should be paid more attention on the optimal extent of aggregation and miscibility, which could be distinct for the different polymer/ITIC pairs.

The molecular stacking, distances, orientation and crystallinity in the film state can efficiently affect the photovoltaic properties. And in order to elucidate the relationship between the morphology information and the photovoltaic parameters

with as cast or SVA treatment, the microstructure features of these polymer:ITIC blend films were carefully investigated by 2D GIWAXS method. The diffraction images and the corresponding IP and OOP line cut profiles were shown in **Figure 8**. For as cast films, it was found that the π–π (010) stacking diffractions of PTBD-BZ:ITIC, PTBD-BDD:ITIC, PTBD-FBT:ITIC, and PTBD-Tz:ITIC films mainly appeared along the out of plane direction and corresponding (100) stacking in IP direction, indicating predominant face-on orientation in the blend films. The (010) peaks of the blend films PTBD-BZ:ITIC, PTBD-BDD:ITIC, PTBD-FBT:ITIC, and PTBD-Tz:ITIC are located at 16.82, 16.91, 16.74, and 16.96 nm^{-1}, corresponding to the π–π stacking distance of 3.73, 3.71, 3.75, and 3.70 Å, which was slightly larger than the pure polymers. The π–π stacking peaks of polymers and ITIC merged together and were hard to be separated. The (100) scattering was a mix diffraction ring combination of both the polymer and ITIC. Compared with the GIWAXS result of ITIC, the (100) scattering from polymers can be distinguished (ITIC molecule showed a (100) stacking at 3.7 Å^{-1}).[50] The crystal coherence length (CCL) in this direction was estimated to be 7.2, 9.3, 7.8, and 6.5 nm for PTBD-BZ, PTBD-BDD, PTBD-FBT, and PTBD-Tz, respectively. When SVA treatment was utilized, the four blend films still maintain the above stacking orientation in combination with high ordered lamellar stacking peaks. The π–π stacking distances of the blend films PTBD-BZ:ITIC, PTBD-BDD:ITIC, PTBD-FBT:ITIC, and PTBD-Tz:ITIC were estimated to be 3.62, 3.64, 3.66, and 3.63 Å, closer than those of as-cast films, which could increase the intermolecular charge transport in the vertical direction and readjust phase separation. However, it was found that the crystallinity would be changed and the degree of the crystallinity was totally distinctive for different BHJ blends. As for PTBD-BZ:ITIC blend system, there was no obvious change in (100) crystalline peak with the CCL of 7.5 nm, indicating that PTBD-BZ:ITIC blending can almost maintain unchanged microphase separation which accounts for realizing high performance with or without post treatment. Conversely, the SVA treatment can significantly enhance the

**ADVANCED
SCIENCE NEWS**

www.advancedsciencenews.com

**ADVANCED
ENERGY
MATERIALS**

www.advenergymat.de
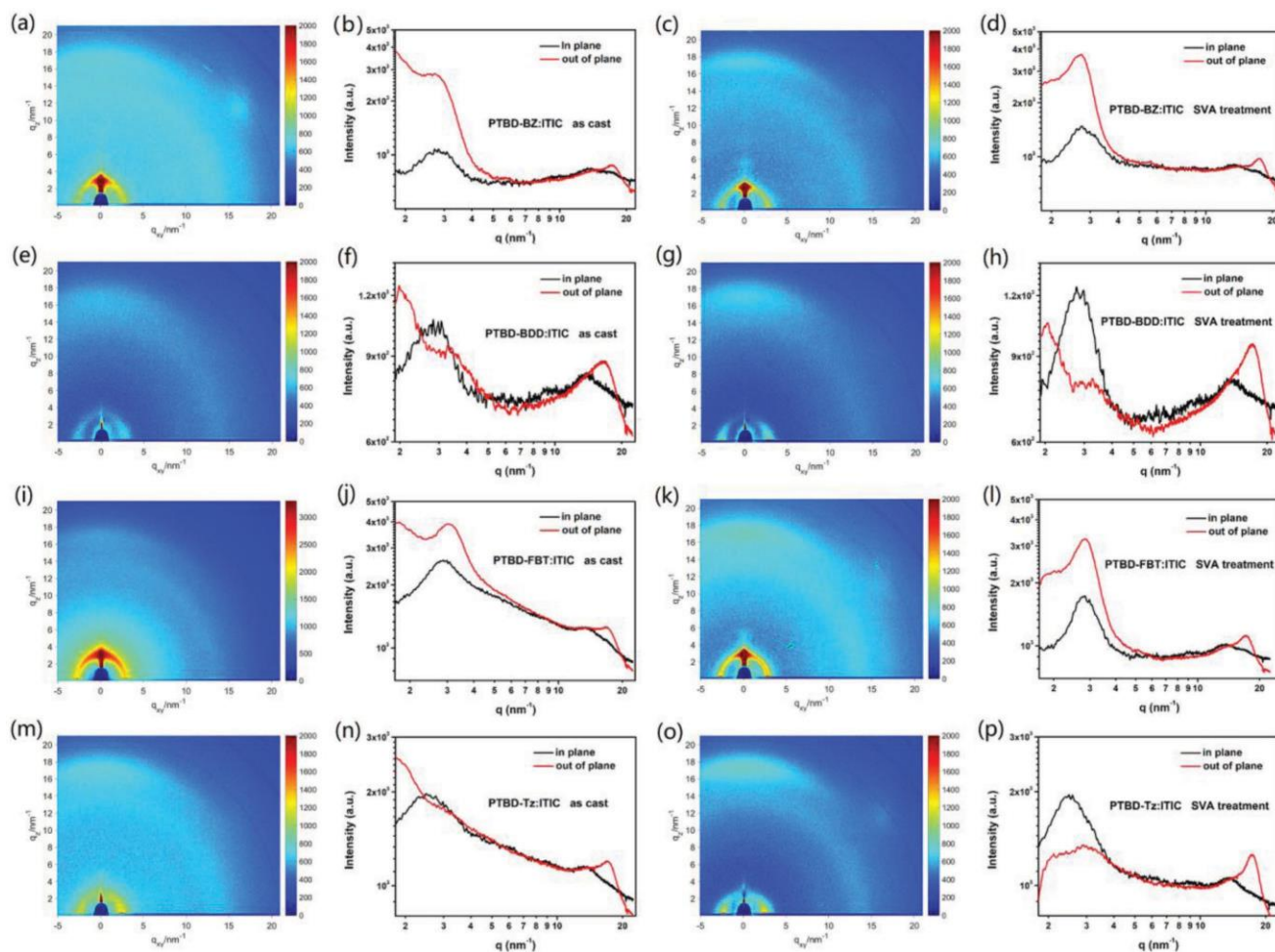
Figure 8. 2D GIWAXS patterns and the line-cut profiles of the polymer:ITIC blend films: a,b) as cast PTBD-BZ:ITIC film; c,d) SVA treatment PTBD-BZ:ITIC film; e,f) as cast PTBD-BDD:ITIC film; g,h) SVA treatment PTBD-BDD:ITIC film; i,j) as cast PTBD-FBT:ITIC film; k,l) SVA treatment PTBD-FBT:ITIC film; m,n) as cast PTBD-Tz:ITIC film; o,p) SVA treatment PTBD-Tz:ITIC film.

crystallinity of PTBD-BDD:ITIC, PTBD-FBT:ITIC, and PTBD-Tz:ITIC as evidenced by the stronger and sharper $\pi-\pi$ stacking peaks as well as the narrower range of (100) scattering angles. The CCL of PTBD-BDD, PTBD-FBT, and PTBD-Tz increased to 11.2, 9.0 and 8.6 nm, resulting in the variational performance of the corresponding devices. The PTBD-BDD:ITIC film with SVA treatment exhibited highly crystallinity and may be prone to form excessive aggregation, thus reducing the *FF* and PCE of the PSCs. However, the PTBD-FBT:ITIC and PTBD-Tz:ITIC films with SVA treatment can modulate the crystallinity to form moderate aggregation and close $\pi-\pi$ stacking, resulting in high J_{SC} and *FF* of the PSCs. The 2D GIWAXS results were quite accordant with the TEM images and reasonable to explain the relationship between the microstructure and photovoltaic performance. Therefore, it can be concluded that first TBD-based pure polymer and polymer/ITIC blend film presented a predominant face on orientation with moderate $\pi-\pi$ stacking distance which has been confirmed to exhibit great advantage in PSCs. Second, for different donor polymer/ITIC pairs, the optimal extent of crystallinity is different. Optimizing crystallinity of the blend film is meant to modulate the aggregation and phase separation,

as well as the miscibility of the D/A pairs. What's more, SVA treatment is an effective method to control the crystallinity and $\pi-\pi$ stacking distance for TBD-based blend films, which can dramatically influence the photovoltaic performance.

3. Conclusion

In summary, the new asymmetric backbone TBD with four aromatic rings was successfully designed and then four polymers PTBD-BZ, PTBD-BDD, PTBD-FBT, and PTBD-Tz with different acceptor units were synthesized to investigate the universality and compatibility of TBD-based polymer in nonfullerene PSCs. On the one hand, the extended conjugation fused-ring aromatic backbone of the polymers can guarantee effective charge carrier transport to obtain large J_{SC}. On the other hand, the asymmetric backbone with two distinct flanked twist angles dramatically affects the polymer geometric configuration and reduces the steric hindrance of the adjacent side chain, which can feasibly modulate the aggregation and crystallinity. Photovoltaic devices based on wide bandgap polymers PTBD-BZ and PTBD-BDD

ADVANCED
SCIENCE NEWS

www.advancedsciencenews.com

ADVANCED
ENERGY
MATERIALS

www.advenergymat.de

achieved the power conversion efficiencies as high as 12.02% and 11.39% without any processing additive or post-treatment. More excitingly, a PCE of 11.02% with a high V_{OC} of 1.02 V and a remarkable J_{SC} of 17.54 mA cm^{-2} was obtained for PTBD-Tz-based device, suggesting that it is feasible to overcome the tradeoff between V_{OC} and J_{SC} and simultaneously obtain high J_{SC} and V_{OC} over 1 V. Our results demonstrate that asymmetric TBD backbone is an excellent moiety to construct light-harvesting copolymers for highly efficient PSCs. Through further optimizing the side chains and acceptor units, the PSCs with even higher efficiency and larger V_{OC} may be envisioned.

Supporting Information

Supporting Information is available from the Wiley Online Library or from the author.

Conflict of Interest

The authors declare no conflict of interest.

[1] G. Yu, J. Gao, J. C. Hummelen, F. Wudl, A. J. Heeger, *Science* **1995**, *270*, 1789.

[2] A. C. Arias, J. D. Mackenzie, I. Mcculloch, J. Rivnay, A. Salleo, *Chem. Rev.* **2010**, *110*, 3.

[3] G. Li, R. Zhu, Y. Yang, *Nat. Photonics* **2012**, *6*, 153.

[4] N. Espinosa, M. Hösel, M. Jørgensen, F. C. Krebs, *Energy Environ. Sci.* **2014**, *7*, 855.

[5] P. Cheng, G. Li, X. Zhan, Y. Yang, *Nat. Photonics* **2018**, *12*, 131.

[6] W. Zhao, S. Li, H. Yao, S. Zhang, Z. Yun, Y. Bei, J. Hou, *J. Am. Chem. Soc.* **2017**, *139*, 7148.

[7] H.-H. Gao, Y. Sun, X. Wan, X. Ke, H. Feng, B. Kan, Y. Wang, Y. Zhang, C. Li, Y. Chen, *Adv. Sci.* **2018**, *5*, 1800307.

[8] Z. Xiao, X. Jia, L. Ding, *Sci. Bull.* **2017**, *62*, 1562.

[9] S. Li, L. Ye, W. Zhao, H. Yan, B. Yang, D. Liu, W. Li, H. Ade, J. Hou, *J. Am. Chem. Soc.* **2018**, *140*, 7159.

[10] Y. Huang, E. J. Kramer, A. J. Heeger, G. C. Bazan, *Chem. Rev.* **2014**, *114*, 7006.

[11] L. Ye, H. Hu, M. Ghasemi, T. Wang, B. A. Collins, J. H. Kim, K. Jiang, J. H. Carpenter, H. Li, Z. Li, T. McAfee, J. Zhao, X. Chen, J. L. Y. Lai, T. Ma, J. L. Bredas, H. Yan, H. Ade, *Nat. Mater.* **2018**, *17*, 253.

[12] Y. Lin, F. Zhao, Y. Wu, K. Chen, Y. Xia, G. Li, S. K. Prasad, J. Zhu, L. Huo, H. Bin, Z. G. Zhang, X. Guo, M. Zhang, Y. Sun, F. Gao, Z. Wei, W. Ma, C. Wang, J. Hodgkiss, Z. Bo, O. Inganas, Y. Li, X. Zhan, *Adv. Mater.* **2017**, *29*, 1604155.

[13] C. Yan, S. Barlow, Z. Wang, H. Yan, A. K. Jen, S. R. Marder, X. Zhan, *Nat. Rev. Mater.* **2018**, *3*, 18003.

[14] S. Dai, F. Zhao, Q. Zhang, T. Lau, T. Li, K. Liu, Q. Ling, C. Wang, X. Lu, W. You, X. Zhan, *J. Am. Chem. Soc.* **2017**, *139*, 1336.

[15] J. Wang, J. Zhang, Y. Xiao, T. Xiao, R. Zhu, C. Yan, Y. Fu, G. Lu, X. Lu, S. R. Marder, X. Zhan, *J. Am. Chem. Soc.* **2018**, *140*, 9140.

[16] J. Sun, X. Ma, Z. Zhang, J. Yu, J. Zhou, X. Yin, L. Yang, R. Geng, R. Zhu, F. Zhang, W. Tang, *Adv. Mater.* **2018**, *30*, 1707150.

[17] H. Bin, L. Gao, Z. G. Zhang, Y. Yang, Y. Zhang, C. Zhang, S. Chen, L. Xue, C. Yang, M. Xiao, Y. Li, *Nat. Commun.* **2016**, *7*, 13651.

[18] A. Tang, B. Xiao, Y. Wang, F. Gao, K. Tajima, H. Bin, Z.-G. Zhang, Y. Li, Z. Wei, E. Zhou, *Adv. Funct. Mater.* **2018**, *28*, 1704507.

[19] D. Baran, T. Kirchartz, S. Wheeler, S. Dimitrov, M. Abdelsamie, J. Gorman, R. S. Ashraf, S. Holliday, A. Wadsworth, N. Gasparini, P. Kaienburg, H. Yan, A. Amassian, C. J. Brabec, J. R. Durrant, I. McCulloch, *Energy Environ. Sci.* **2016**, *9*, 3783.

[20] L. Ye, W. Zhao, S. Li, S. Mukherjee, J. H. Carpenter, O. Awartani, X. Jiao, J. Hou, H. Ade, *Adv. Energy Mater.* **2017**, *7*, 1602000.

[21] S. Li, L. Ye, W. Zhao, X. Liu, J. Zhu, H. Ade, J. Hou, *Adv. Mater.* **2017**, *29*, 1704051.

[22] S. Feng, C. Zhang, Y. Liu, Z. Bi, Z. Zhang, X. Xu, W. Ma, Z. Bo, *Adv. Mater.* **2017**, *29*, 1703527.

[23] H. Yao, L. Ye, J. Hou, B. Jang, G. Han, Y. Cui, G. M. Su, C. Wang, B. Gao, R. Yu, H. Zhang, Y. Yi, H. Y. Woo, H. Ade, J. Hou, *Adv. Mater.* **2017**, *29*, 1700254.

[24] X. Xu, T. Yu, Z. Bi, W. Ma, Y. Li, Q. Peng, *Adv. Mater.* **2018**, *30*, 1703973.

[25] D. Liu, B. Yang, B. Jang, B. Xu, S. Zhang, C. He, H. Y. Woo, J. Hou, *Energy Environ. Sci.* **2017**, *10*, 546.

[26] H. Bin, Z. G. Zhang, L. Gao, S. Chen, L. Zhong, L. Xue, C. Yang, Y. Li, *J. Am. Chem. Soc.* **2016**, *138*, 4657.

[27] Y. Lin, Q. He, F. Zhao, L. Huo, J. Mai, X. Lu, C. Su, T. Li, J. Wang, J. Zhu, Y. Sun, C. Wang, X. Zhan, *J. Am. Chem. Soc.* **2016**, *138*, 2973.

[28] X. Bao, Y. Zhang, J. Wang, D. Zhu, C. Yang, Y. Li, C. Yang, J. Xu, R. Yang, *Chem. Mater.* **2017**, *29*, 6766.

[29] P. Gao, J. Tong, P. Guo, J. Li, N. Wang, C. Li, X. Ma, P. Zhang, C. Wang, Y. Xia, *J. Polym. Sci., Part A: Polym. Chem.* **2018**, *56*, 85.

[30] Y. Lin, F. Zhao, Q. He, L. Huo, Y. Wu, T. C. Parker, W. Ma, Y. Sun, C. Wang, D. Zhu, A. J. Heeger, S. R. Marder, X. Zhan, *J. Am. Chem. Soc.* **2016**, *138*, 4955.

[31] L. Ye, S. Zhang, L. Huo, M. Zhang, J. Hou, *Acc. Chem. Res.* **2014**, *47*, 1595.

[32] Q. Fan, W. Su, X. Guo, Y. Wang, J. Chen, C. Ye, M. Zhang, Y. Li, *J. Mater. Chem. A* **2017**, *5*, 9204.

[33] X. Wang, J. Tong, P. Guo, Y. Li, H. Li, Y. Xia, F. Wang, *Polymer* **2017**, *122*, 96.

[34] L. Huo, T. Liu, X. Sun, Y. Cai, A. J. Heeger, Y. Sun, *Adv. Mater.* **2015**, *27*, 2938.

[35] Y. Wu, Z. Li, W. Ma, Y. Huang, L. Huo, X. Guo, M. Zhang, H. Ade, J. Hou, *Adv. Mater.* **2013**, *25*, 3449.

[36] D. Liu, J. Wang, C. Gu, Y. Li, X. Bao, R. Yang, *Adv. Mater.* **2018**, *30*, 1705870.

[37] Y. Wang, Z. Yan, H. Guo, M. Uddin, S. Ling, X. Zhou, H. Su, J. Dai, H. Woo, X. Guo, *Angew. Chem., Int. Ed.* **2017**, *56*, 15304.

[38] C. Cui, W. Y. Wong, Y. Li, *Energy Environ. Sci.* **2014**, *7*, 2276.

[39] Y. Lin, J. Wang, Z. G. Zhang, H. Bai, Y. Li, D. Zhu, X. Zhan, *Adv. Mater.* **2015**, *27*, 1170.

[40] J. W. Jo, J. W. Jung, H.-W. Wang, P. Kim, T. P. Russell, W. H. Jo, *Chem. Mater.* **2014**, *26*, 4214.

[41] D. Zhu, X. Bao, Q. Zhu, C. Gu, M. Qiu, S. Wen, J. Wang, B. Shahid, R. Yang, *Energy Environ. Sci.* **2017**, *10*, 614.

[42] T. Liu, X. Pan, X. Meng, Y. Liu, D. Wei, W. Ma, L. Huo, X. Sun, T. H. Lee, M. Huang, H. Choi, J. Y. Kim, W. C. Choy, Y. Sun, *Adv. Mater.* **2016**, *1604251*.

[43] C. M. Cardona, W. Li, A. E. Kaifer, D. Stockdale, G. C. Bazan, *Adv. Mater.* **2011**, *23*, 2367.

[44] W. Zhang, C. Song, Y. Li, X. Liu, X. Wang, X. Sun, J. Fang, *Org. Electron.* **2017**, *47*, 94.

[45] C. Gu, Z. Zhang, S. Sun, Y. Pan, C. Zhong, Y. Lv, M. Li, K. Ariga, F. Huang, Y. Ma, *Adv. Mater.* **2012**, *24*, 5727.

[46] Y. Shirota, M. Kinoshita, T. Noda, K. Okumoto, T. Ohara, *J. Am. Chem. Soc.* **2000**, *122*, 11021.

[47] B. Liu, X. Chen, Y. Zou, L. Xiao, X. Xu, L. He, Y. Li, *Macromolecules* **2012**, *45*, 6898.

[48] G. Li, V. Shrotriya, J. Huang, Y. Yao, T. Moriarty, K. Emery, Y. Yang, *Nat. Mater.* **2005**, *4*, 864.

[49] N. D. Treat, M. L. Chabinyc, *Annu. Rev. Phys. Chem.* **2014**, *65*, 59.

[50] L. Gao, Z. G. Zhang, H. Bin, L. Xue, Y. Yang, C. Wang, F. Liu, T. P. Russell, Y. Li, *Adv. Mater.* **2016**, *28*, 8288.